Highly Sensitive Diagnostic Assay for the Detection of Protein Biomarkers Using Microresonators and Multifunctional Nanoparticles

Jinmyoung Joo, Donghoon Kwon, Changyong Yim, and Sangmin Jeon*

Department of Chemical Engineering, Pohang University of Science and Technology (POSTECH), Pohang, Korea

ABSTRACT

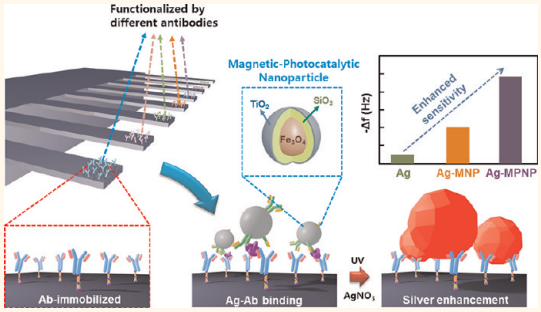

We developed a novel gravimetric immunoassay for sensitive detection of multiple protein biomarkers using silicon microcantilever arrays and multifunctional hybrid nanoparticles. Magnetic—photocatalytic hybrid nanoparticles with a highly crystalline TiO_2 shell were synthesized using a solvothermal reaction without a calcination process. After functionalizing the hybrid nanoparticles and silicon cantilevers with antibodies, the nanoparticles were used to magnetically separate target biomarkers from human serum. Frequency changes of the microcantilevers due to the binding of the nanoparticles were measured using a dip-and-dry method. Frequency changes were further amplified using a photocatalytic silver reduction reaction. Several biomarkers, including interleukin-6, interferon-γ, and alpha-fetoprotein, were selectively detected using arrays of eight silicon microcantilevers. The detection limit of this assay was ~0.1 pg/mL, which is superior to the clinical threshold of the biomarkers.

KEYWORDS: immunoassay · microresonators · photocatalyst · magnetic nanoparticles

Rapid, sensitive, and high-throughput detection of disease biomarkers in human serum is a critical clinical issue, because the concentrations of protein biomarkers are generally associated with certain disease processes.[1,2] Thus, the early detection of disease-related proteins using ultrasensitive methods can save lives and money. The required sensitivity for typical cancer biomarkers is 1 ng/mL, whereas the detection of cytokines such as interleukins (ILs) and interferon (INF)-γ requires a higher sensitivity (~1 pg/mL) due to lower thresholds.[2−4] Although conventional immunoassay methods, including enzyme-linked immunosorbent assays (ELISA) and fluorescence immunoassays, can measure the concentrations of disease-related proteins, they have disadvantages, including time-consuming procedures involving expensive instrumentation and complicated separation and labeling steps.

Recent advances in microfabrication and nanotechnology offer the possibilities of highly sensitive, cost-effective assay methods, through the mass production of miniaturized sensors. Cantilever-based microresonators have attracted much interest as candidate next-generation biosensor platforms.[5−12] Microcantilever resonators have advantages for diagnostic applications because they do not require labeling target molecules, and the array structures enable the simultaneous detection of multiple analytes. Although the mass sensitivities of nanocantilevers are incredibly high (better than 1 atto-gram in a vacuum),[13] handling nanocantilevers during preparation and measurement steps is not easy. Integrated microcantilever resonators (*i.e.*, piezoelectric microcantilevers) with very high resonance frequencies may be a good alternative, but their fabrication is complicated and cost-ineffective.[14]

We have developed a new assay system, consisting of commercially available plain silicon microcantilevers that are both economical and easy to handle. In this system, resonance frequency changes are amplified by magnetic preconcentration and photocatalytic silver enhancement reactions. Antibody-conjugated magnetic nanoparticles are used for magnetic preconcentration

* Address correspondence to jeons@postech.ac.kr.

Received for review March 12, 2012 and accepted April 20, 2012.

Published online April 20, 2012
10.1021/nn301071c

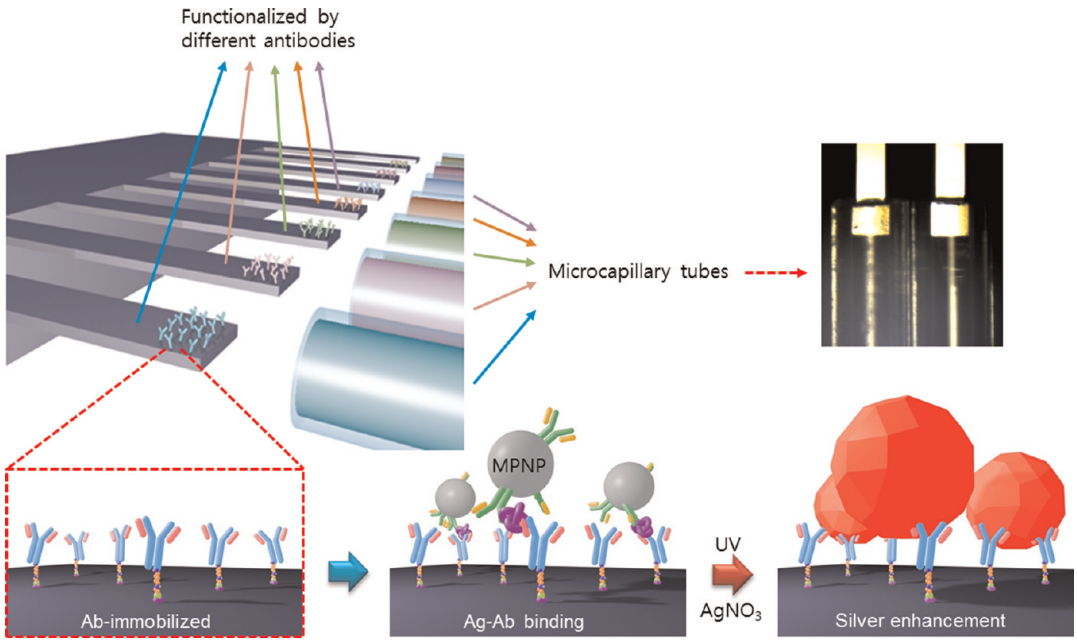

Figure 1. Schematic illustration of a hybrid nanoparticle-based sandwich immunoassay with photocatalytic reduction of silver.

to separate target analytes from a complex medium under an external magnetic field. Photocatalytic silver enhancement uses photocatalytic nanoparticles to reduce silver ions to metallic silver. The deposition of silver on the nanoparticles increases their mass, resulting in greater frequency changes of the microcantilever sensors. Because silver is reduced only around the nanoparticles under UV irradiation, the reduction reaction is easier to control and more reproducible than conventional silver reduction reactions based on gold nanoparticles, which occur not only around the gold nanoparticles but also in solution.[15]

To implement the simultaneous magnetic preconcentration and photocatalytic silver reduction, we utilize a solvothermal process to synthesize magnetic–photocatalytic hybrid nanoparticles. The Fe_3O_4 core enables the preconcentration of target proteins, and the TiO_2 shell enables the photocatalytic reduction of silver. The binding of antibody-conjugated hybrid nanoparticles to the cantilevers and the subsequent photocatalytic deposition of silver increase the mass of the nanoparticles, enhancing the sensitivity of the microcantilever resonators (Figure 1). To our knowledge, this paper is the first to report the synthesis of highly crystalline TiO_2 shells on magnetic cores without a calcination process and the first application of multifunctional hybrid nanoparticles to microcantilever sensors to detect very low concentrations (0.1 pg/mL) of multiple protein biomarkers in human serum.

RESULTS AND DISCUSSION

Magnetic nanoparticles with a narrow size distribution were synthesized using a one-pot solvothermal method, as described previously,[16,17] and SiO_2 shells were prepared using the Stöber method.[18] Although various methods have been used to synthesize magnetic–photocatalytic nanoparticles,[19–22] preparation of highly crystalline TiO_2 shells without calcination remains challenging. Because heat treatment for the crystallization of TiO_2 can cause the nanoparticles to aggregate, the TiO_2 shells are temporarily coated with SiO_2 layers and removed after calcination.[23] Although this scheme works in the production of crystalline TiO_2 shells, it is not convenient to coat and etch the SiO_2 layers. We therefore developed a direct solvothermal method of producing highly crystalline TiO_2 shells, without calcination.

Fe_3O_4@SiO_2 solution in ethanol (2 mL) was diluted into 50 mL of ethanol and dispersed by sonication. To this solution were added 300 μL of deionized water and 150 μg of hydroxypropyl cellulse (surfactant) while stirring continuously, after which the mixture was transferred to a Teflon-lined autoclave. Then 200 μL of tetrabutyl titanate dissolved in excess acetylacetonate was mixed with 5 mL of absolute ethanol, and the solution was added dropwise to the Fe_3O_4@SiO_2 solution. In the absence of acetylacetonate, titanium precursors are hydrolyzed very quickly, resulting in aggregation of the particles to form peapod-like structures.[24] In the presence of acetylacetonate, however, the hydrolysis reaction rate is reduced due to the strong ionic interaction between Ti^{4+} and acetylacetonate, producing isolated core@shell nanoparticles.

The autoclave was sealed and heated to 180 °C for 10 h with vigorous stirring. After natural cooling to room temperature, the final products were washed several times with ethanol and redispersed in ethanol or distilled water. Note that the crystalline TiO_2 shells

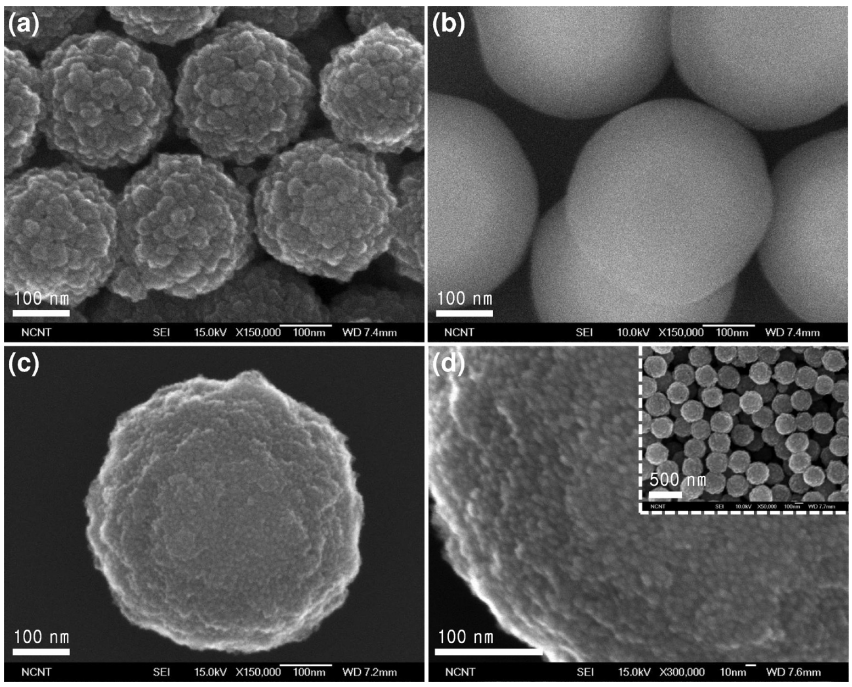

Figure 2. Scanning electron microscope (SEM) images of (a) Fe_3O_4, (b) Fe_3O_4@SiO_2, and (c) Fe_3O_4@SiO_2@TiO_2. (d) Magnified image of (c).

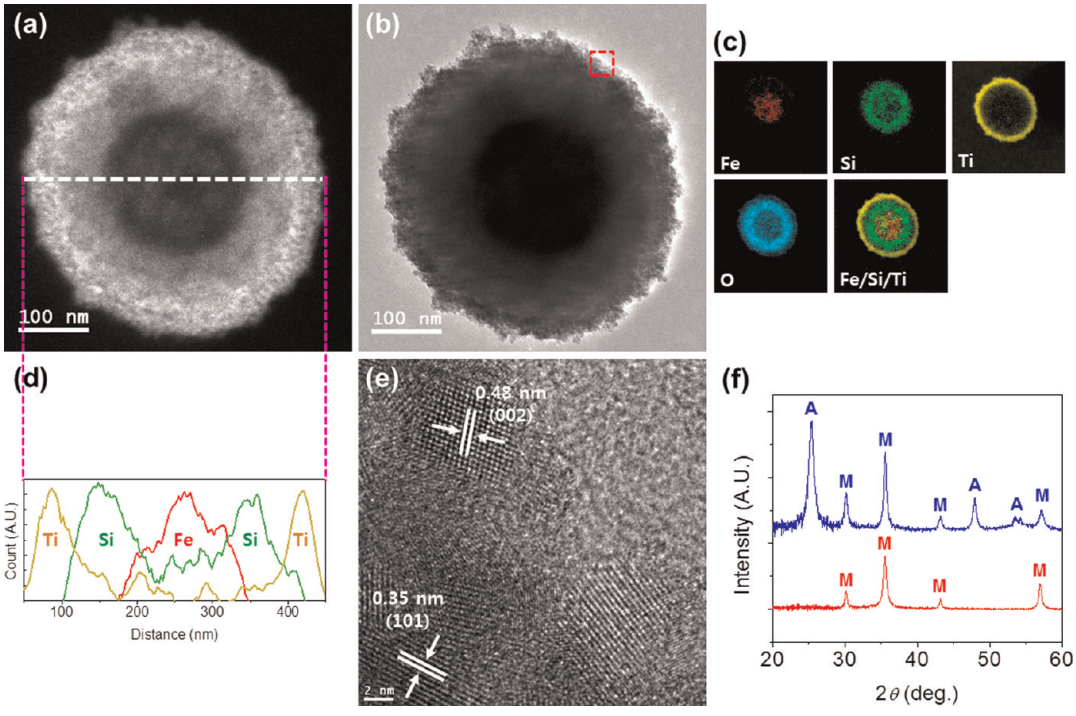

Figure 3. (a) Dark field STEM and (b) TEM images of Fe_3O_4@SiO_2@TiO_2 nanoparticles. (c) Elemental mappings of Fe_3O_4@SiO_2@TiO_2 nanoparticles. (d) Cross-sectional elemental profiles of Fe_3O_4@SiO_2@TiO_2 nanoparticles. (e) High-resolution TEM image of TiO_2 shells in the region marked in (b). (f) X-ray diffraction patterns of as-synthesized Fe_3O_4 (red) and Fe_3O_4@SiO_2@TiO_2 (blue) nanoparticles (A: anatase, M: magnetite).

were obtained by a one-step solvothermal process without postheat treatment. To our knowledge, this is the first description of the synthesis of crystalline TiO_2 shells without calcinations.

Figure 2a shows an SEM image of Fe_3O_4 nanoparticles with a mean diameter of 180 nm. These nanoparticles are composed of small primary nanocrystals (~15 nm in diameter), which possess superparamagnetic properties. The magnetic separation efficiency increases along with the size of the magnetic nanoparticles, but Fe_3O_4 nanoparticles larger than 30 nm tend to assume ferromagnetic properties.[25] Figure 2b and c show SEM

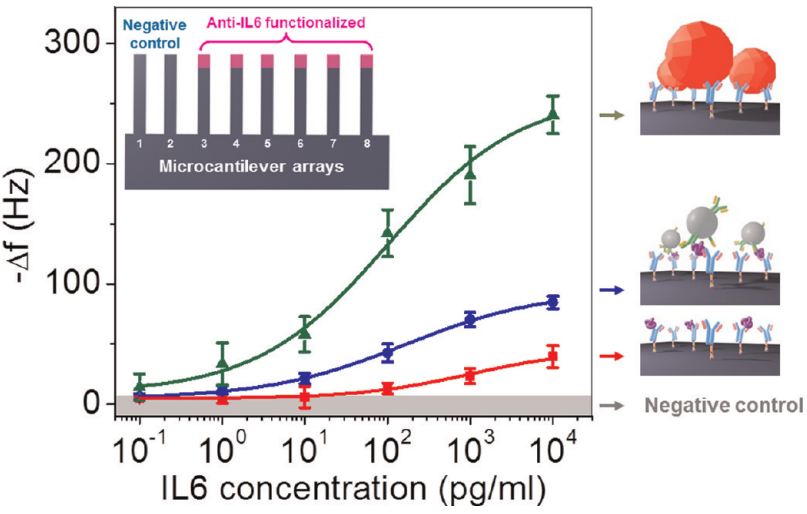

Figure 4. Changes in resonance frequency of the cantilever arrays due to the binding of an antigen (red), an MPNP-bound antigen after magnetic separation (blue), and silver-enhanced MPNP (green). The gray box represents the differences in frequency from the reference cantilevers. The inset shows a schematic of the IL6-antibody-functionalized microcantilever array.

TABLE 1. Comparison of the Sensitivities of Various Microcantilever Sensors in the Detection of Proteins Using Dip-and-Dry Assay Techniques

cantilever type	resonance frequency	analyte	mass enhancement	limit of detection
piezoresistive[30]	100 kHz	alpha-fetoprotein		2 ng/mL
piezoelectric[31]	1.3 MHz	hepatitis B virus		0.1 ng/mL
piezoelectric[32]	68 kHz	hepatitis C virus		0.1 ng/mL
piezoelectric[33]	90 kHz	prostate specific antigen	silica nanoparticles	1 pg/mL
plain silicon[34,35]	4.6 MHz (vacuum)	prion proteins	magnetic nanoparticles	0.2 ng/mL
plain silicon (this work)	27 kHz	interleukin-6	magnetic–photocatalytic hybrid nanoparticles	0.1 pg/mL

images of Fe_3O_4@SiO_2 and Fe_3O_4@SiO_2@TiO_2 nanoparticles, respectively. Silica layers were introduced between Fe_3O_4 and TiO_2 to prevent the photodissolution of Fe_3O_4 during the photocatalytic reaction.[26] The smooth surface of Fe_3O_4@SiO_2 nanoparticles became rough after coating with TiO_2 layers. The high-magnification SEM image in Figure 2d demonstrates that self-assembled TiO_2 nanocrystal clusters formed on the Fe_3O_4@SiO_2 nanoparticles during a solvothermal reaction. The increased surface area of magnetic–photocatalytic nanoparticles (MPNPs) due to the TiO_2 nanocrystals enhanced the subsequent immunoreaction and photocatalytic activity. The size of MPNPs was quite uniform, with no aggregation observed (Figure 2d, inset).

The microstructures of the MPNPs were further investigated by transmission electron miscroscopy (TEM). The dark field STEM and TEM images of MPNPs in Figure 3a and b, respectively, show the presence of a core@shell@shell structure. The thicknesses of the SiO_2 and TiO_2 were ~70 and ~30 nm, respectively. The corresponding elemental mappings and cross-sectional profiles obtained by electron energy loss spectroscopy confirmed that the MPNPs consisted of Fe_3O_4@SiO_2@TiO_2 (Figure 3c and d). Figure 3e shows a high-resolution TEM image of the marked region in Figure 3b, confirming that the TiO_2 shell consists of crystalline nanoparticles. The crystal structure of the MPNPs was further investigated by X-ray diffraction (XRD), with the diffraction peaks in Figure 3f indexed to the magnetite phase of Fe_3O_4 (JCPDS 89-0691) and the anatase phase of TiO_2 (JCPDS 84-1285). Because the SiO_2 interlayer is amorphous, it had no characteristic peaks. The Debye–Scherrer equation indicated that the TiO_2 nanocrystals averaged ~8.5 nm in size,[27] consistent with the results obtained from the HR-TEM images.

Figure 4 shows variations in the resonance frequency of the cantilever arrays due to the binding of IL-6 and subsequent reduction of silver on the cantilevers. The mass change (Δm) due to the binding of IL-6 and subsequent silver deposition can be calculated from the frequency change (Δf) as

$$\Delta m = \frac{k}{4\pi^2}\left(\frac{1}{f_1^2} - \frac{1}{f_0^2}\right) \quad (1)$$

where f_0 and f_1 are the initial frequency and the frequency after mass loading, respectively. Because mass was loaded only at the free end of the cantilevers, we neglected the effects of adsorption-induced surface stress on the spring constant of the cantilevers.[28,29]

The schematic inset in Figure 4 shows how each cantilever was functionalized using specific antibodies.

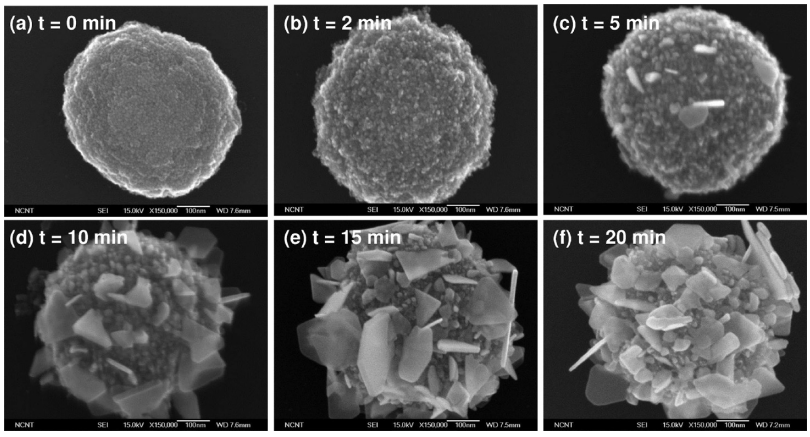

Figure 5. SEM images of an Fe_3O_4@SiO_2@TiO_2 nanoparticle as a function of photocatalytic silver reduction reaction time: (a) 0 min, (b) 2 min, (c) 5 min, (d) 10 min, (e) 15 min, and (f) 20 min.

Two cantilevers treated with BSA to suppress the nonspecific binding of IL-6 were used as reference cantilevers. The other six cantilevers were functionalized with BSA and antibodies to IL-6 using microcapillary tubes and used to assess specific antigen–antibody binding. Twelve cantilever arrays were prepared, and each array was incubated for 1 h in human serum spiked with 0.1 pg/mL to 10 ng/mL IL-6. Changes in resonance frequency increased with IL-6 concentration, whereas the reference cantilevers showed a negligible frequency shift. The sensitivity of the cantilevers before MPNP binding (~1000 pg/mL) was increased after photocatalytic enhancement to ~0.1 pg/mL, far higher than the clinical threshold (~6 pg/mL).[4] Table 1 shows the sensitivities of various microcantilever sensors in the detection of proteins using dip-and-dry methods.[30–35] Although the resonance frequency of the microcantilever in this study is lower than those in the references, its limit of detection is superior to the reported values due to the utilization of the hybrid nanoparticles for magnetic preconcentration and photocatalytic mass enhancement.

Figure 5 shows a series of SEM images of silver-deposited MPNPs as a function of photocatalytic silver reduction time. At the beginning of silver reduction, small silver nanospheres formed on TiO_2 surfaces due to the reduction of silver ions by photogenerated electrons (Figure 5b). As the silver reduction reaction continued, the silver nanospheres grew to silver nanoplates (Figure 5c–f). Photoinduced fragmentation and ripening processes were reported to be responsible for the conversion of silver nanospheres to triangular nanoprisms.[36,37] The nonuniform growth of metallic silver may be due to the trapping of photogenerated electrons on metallic silver present on the surface of TiO_2, resulting in a more rapid and favorable reduction of silver ions on silver-deposited sites.

To apply our assay in the detection of multiple biomarkers, two microcantilevers each were functionalized with antibodies to IL-6, IFN-γ, and AFP (Figure 6). The remaining two cantilevers were treated with BSA and used as references. Each of the eight cantilever arrays was incubated in a solution containing preconcentrated single antigen or multiple antigens. The original concentration of each antigen solution was 1 pg/mL in human serum and preconcentrated using antibody-functionalized MPNPs. Figure 6 shows changes in the resonance frequency of the microcantilevers after photocatalytic silver enhancement. The reference cantilevers showed negligible changes in frequency (within experimental error), whereas the six other cantilevers showed large frequency changes specific to the antigen in each solution. The three antigens were successfully detected within 1 h, with the sensitivity of detection being much higher than that of competing techniques, including conventional ELISA, fluorescent microarray, and electrochemical methods.[38–42]

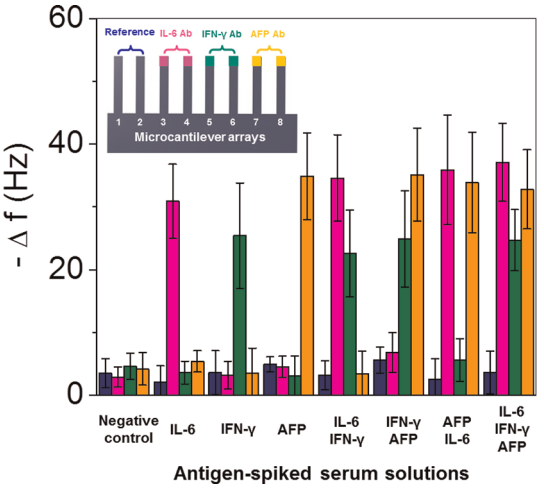

Figure 6. Changes in the resonance frequency of each cantilever after binding of various protein biomarkers (1 pg/mL in serum) and photocatalytic silver enhancement. (navy: reference, pink: IL-6, green: IFN-γ, orange: AFP) The inset shows a schematic representation of the multiple antibody-functionalized microcantilever array.

CONCLUSION

In summary, we have developed a novel immunoassay, using a combination of multifunctional hybrid nanoparticles and microcantilever arrays. The magnetic–photocatalytic hybrid nanoparticles, with high magnetization and crystalline structure, were synthesized using a simple solvothermal process without postcalcination and used to separate target antigens from human serum. After binding of the MPNPs to the cantilevers, the change in frequency was amplified by the photocatalytic reduction of silver. The limit detection of our assay was 0.1 pg/mL, which is superior to that of conventional ELISA techniques. In addition, the short assay time (~1 h) and ability to detect several antigens suggest that this method may be a promising alternative to conventional techniques in clinical applications.

MATERIALS AND METHODS

Materials. 3-Aminopropyltriethoxysilane (APTES), absolute ethanol, bovine serum albumin (BSA), $FeCl_3$, polyacrylamide, urea, sodium citrate, silver nitrate, tetraethyl orthosilicate (TEOS), ammonium hydroxide, hydroxypropyl cellulose (HPC), acetylacetonate, tetrabutyl titanate (TBOT), dimethyl sulfoxide (DMSO), glutaraldehyde, and human sera were purchased from Sigma-Aldrich and used without further purification. Human IL-6, IFN-γ, and alpha-fetoprotein (AFP), and antibodies against each, were purchased from BD Bioscience (CA, USA). Deionized water (18.3 MΩ cm^{-1}) was prepared using a reverse osmosis water system and was used to prepare phosphate buffer (10 mM).

Synthesis of Fe_3O_4 Nanoparticles. Magnetic nanoparticles with a narrow size distribution were synthesized using a one-pot solvothermal method, as described previously.[16,17] Briefly, 4 mmol of $FeCl_3$, 12 mmol of urea, and 8 mmol of sodium citrate were dissolved in 80 mL of water, to which was added 0.6 g of polyacrylamide (7.5 g/L) under continuous stirring. The solution was transferred to a 100 mL Teflon-lined autoclave, which was sealed and maintained at 200 °C for 12 h. The solution was naturally cooled to room temperature, and the precipitate was collected using a permanent magnet and washed several times with water and ethanol.

Synthesis of Fe_3O_4@SiO_2 Nanoparticles. SiO_2 shells were prepared using the Stöber method.[18] Briefly, 1 mL of Fe_3O_4 aqueous solution was mixed with 20 mL of ethanol and 1 mL of ammonium hydroxide and sonicated. To the resulting solution was added 0.1 mL of TEOS, followed by agitation for 30 min. The resulting Fe_3O_4@SiO_2 nanoparticles were washed three times with ethanol and redispersed in ethanol.

Characterization of Nanoparticles. The crystalline structure of the nanoparticles was characterized by X-ray diffraction on a M18XHF (Mac Science) diffractometer with Cu Kα radiation (λ = 1.542 Å). The morphology of the nanoparticles was determined by scanning electron microscopy (SEM) on a JEOL JSM-7401F field emission SEM (FE-SEM, 15 kV). The structure and chemical composition of the nanoparticles were investigated using transmission electron microscopy (JEOL JEM-2200FS) with an accelerating voltage of 200 kV.

Detection of Protein Biomarkers. Synthesized MPNPs (0.3 mg/mL) were treated with APTES (1% in ethanol) and glutaraldehyde (5% in distilled water) and washed in buffer solution, and the monoclonal capture antibodies were immobilized onto the nanoparticles. Antibody-functionalized MPNPs were incubated in 1 mL of antigen-spiked serum for 30 min, magnetically separated, and redispersed in 0.1 mL of buffer for preconcentration. Silicon microcantilever arrays were sequentially treated with APTES (1% in ethanol), NHS-LC-biotin (100 μg/mL in DMSO), and streptavidin (0.1 mg/mL).[43] The biotinylated polyclonal antibodies used for detection were functionalized at the free end of each microcantilever using microcapillary tubes (Figure 1), followed by washing with 0.1 mg/mL Tween-20 to overcome the limitation induced by nonspecific binding.[44] The functionalized microcantilever array chips were incubated in preconcentrated solutions for 30 min and dried under nitrogen flow. The resonance frequency of the cantilevers was measured before and after incubation.

For photocatalytic silver reduction, the microcantilever arrays were immersed in a 10 mM $AgNO_3$ solution and exposed to UV light (λ = 254 nm, Spectroline, NY, USA) for 20 min. After rinsing and drying the cantilevers, the resonance frequency was measured by monitoring the frequency spectrum of acoustically actuated cantilevers. An optical method was used to determine the frequency spectrum of each microcantilever.[29] In brief, a focused laser beam was reflected off the free end of each microcantilever onto a position-sensitive detector, and the voltage change due to the vibration of the cantilever was converted to a resonance peak using a fast Fourier transform technique. The resonance peaks were fit with Lorentzian curves, and the corresponding resonance frequencies were calculated. Figure 1 shows a schematic of a hybrid nanoparticle-based sandwich immunoassay with photocatalytic silver reduction.

Conflict of Interest: The authors declare no competing financial interest.

Acknowledgment. This research was supported by the Basic Science Research Program through the National Research Foundation of Korea (NRF) funded by the Ministry of Education, Science and Technology (20110011246).

REFERENCES AND NOTES

1. Ferrari, M. Cancer Nanotechnology: Opportunities and Challenges. *Nat. Rev. Cancer* **2005**, *5*, 161–171.
2. Wu, J.; Fu, Z. F.; Yan, F.; Ju, H. X. Biomedical and Clinical Applications of Immunoassays and Immunosensors for Tumor Markers. *Trends Anal. Chem.* **2007**, *26*, 679–688.
3. Peng, J.; Feng, L. N.; Ren, Z. J.; Jiang, L. P.; Zhu, J. J. Synthesis of Silver Nanoparticle-Hollow Titanium Phosphate Sphere Hybrid as a Label for Ultrasensitive Electrochemical Detection of Human Interleukin-6. *Small* **2011**, *7*, 2921–2928.
4. Malhotra, R.; Patel, V.; Vaque, J. P.; Gutkind, J. S.; Rusling, J. F. Ultrasensitive Electrochemical Immunosensor for Oral Cancer Biomarker IL-6 Using Carbon Nanotube Forest Electrodes and Multilabel Amplification. *Anal. Chem.* **2010**, *82*, 3118–3123.
5. Waggoner, P. S.; Varshney, M.; Craighead, H. G. Detection of Prostate Specific Antigen with Nanomechanical Resonators. *Lab Chip* **2009**, *9*, 3095–3099.
6. Bosco, F. G.; Hwu, E. T.; Chen, C. H.; Keller, S.; Bache, M.; Jakobsen, M. H.; Hwang, I. S.; Boisen, A. High Throughput Label-Free Platform for Statistical Bio-Molecular Sensing. *Lab Chip* **2011**, *11*, 2411–2416.
7. von Muhlen, M. G.; Brault, N. D.; Knudsen, S. M.; Jiang, S. Y.; Manalis, S. R. Label-Free Biomarker Sensing in Undiluted Serum with Suspended Microchannel Resonators. *Anal. Chem.* **2010**, *82*, 1905–1910.
8. Allendorf, M. D.; Houk, R. J. T.; Andruszkiewicz, L.; Talin, A. A.; Pikarsky, J.; Choudhury, A.; Gall, K. A.; Hesketh, P. J. Stress-Induced Chemical Detection Using Flexible Metal-Organic Frameworks. *J. Am. Chem. Soc.* **2008**, *130*, 14404–14405.
9. Ramos, D.; Arroyo-Hernandez, M.; Gil-Santos, E.; Tong, H. D.; Van Rijn, C.; Calleja, M.; Tamayo, J. Arrays of Dual Nanomechanical Resonators for Selective Biological Detection. *Anal. Chem.* **2009**, *81*, 2274–2279.
10. Arlett, J. L.; Myers, E. B.; Roukes, M. L. Comparative Advantages of Mechanical Biosensors. *Nat. Nanotechnol.* **2011**, *6*, 203–215.

11. Gruber, K.; Horlacher, T.; Castelli, R.; Mader, A.; Seeberger, P. H.; Hermann, B. A. Cantilever Array Sensors Detect Specific Carbohydrate-Protein Interactions with Picomolar Sensitivity. *ACS Nano* **2011**, *5*, 3670–3678.
12. Zhang, J.; Lang, H. P.; Huber, F.; Bietsch, A.; Grange, W.; Certa, U.; McKendry, R.; Guntgerodt, H. J.; Hegner, M.; Gerber, C. Rapid and Label-Free Nanomechanical Detection of Biomarker Transcripts in Human RNA. *Nat. Nanotechnol.* **2006**, *1*, 214–220.
13. Li, M.; Tang, H. X.; Roukes, M. L. Ultra-Sensitive NEMS-Based Cantilevers for Sensing, Scanned Probe and Very High-Frequency Applications. *Nat. Nanotechnol.* **2007**, *2*, 114–120.
14. Shekhawat, G.; Tark, S. H.; Dravid, V. P. MOSFET-Embedded Microcantilevers for Measuring Deflection in Biomolecular Sensors. *Science* **2006**, *311*, 1592–1595.
15. Gupta, S.; Huda, S.; Kilpatrick, P. K.; Velev, O. D. Characterization and Optimization of Gold Nanoparticle-Based Silver-Enhanced Immunoassays. *Anal. Chem.* **2007**, *79*, 3810–3820.
16. Chun, C.; Joo, J.; Kwon, D.; Kim, C. S.; Cha, H. J.; Chung, M. S.; Jeon, S. A Facile and Sensitive Immunoassay for the Detection of Alpha-Fetoprotein Using Gold-Coated Magnetic Nanoparticle Clusters and Dynamic Light Scattering. *Chem. Commun.* **2011**, *47*, 11047–11049.
17. Cheng, W.; Tang, K. B.; Qi, Y. X.; Sheng, J.; Liu, Z. P. One-Step Synthesis of Superparamagnetic Monodisperse Porous Fe_3O_4 Hollow and Core-Shell Spheres. *J. Mater. Chem.* **2010**, *20*, 1799–1805.
18. Chen, H. M.; Deng, C. H.; Zhang, X. M. Synthesis of Fe_3O_4@SiO_2@PMMA Core-Shell-Shell Magnetic Microspheres for Highly Efficient Enrichment of Peptides and Proteins for MALDI-ToF MS Analysis. *Angew. Chem., Int. Ed.* **2010**, *49*, 607–611.
19. Ye, M. M.; Zhang, Q.; Hu, Y. X.; Ge, J. P.; Lu, Z. D.; He, L.; Chen, Z. L.; Yin, Y. D. Magnetically Recoverable Core-Shell Nanocomposites with Enhanced Photocatalytic Activity. *Chem.—Eur. J.* **2010**, *16*, 6243–6250.
20. Ao, Y. H.; Xu, J. J.; Fu, D. G.; Ba, L.; Yuan, C. W. Deposition of Anatase Titania onto Carbon Encapsulated Magnetite Nanoparticles. *Nanotechnology* **2008**, *19*, 405604.
21. Chen, F.; Xie, Y. D.; Zhao, J. C.; Lu, G. X. Photocatalytic Degradation of Dyes on a Magnetically Separated Photocatalyst under Visible and UV Irradiation. *Chemosphere* **2001**, *44*, 1159–1168.
22. Wang, C. X.; Yin, L. W.; Zhang, L. Y.; Kang, L.; Wang, X. F.; Gao, R. Magnetic (γ-Fe_2O_3@SiO_2)$_n$@TiO_2 Functional Hybrid Nanoparticles with Actived Photocatalytic Ability. *J. Phys. Chem. C* **2009**, *113*, 4008–4011.
23. Zhang, Q.; Joo, J. B.; Lu, Z. D.; Dahl, M.; Oliveira, D. Q. L.; Ye, M. M.; Yin, Y. D. Self-Assembly and Photocatalysis of Mesoporous TiO_2 Nanocrystal Clusters. *Nano Res.* **2011**, *4*, 103–114.
24. Ye, M. M.; Zorba, S.; He, L.; Hu, Y. X.; Maxwell, R. T.; Farah, C.; Zhang, Q.; Yin, Y. D. Self-Assembly of Superparamagnetic Magnetite Particles into Peapod-Like Structures and Their Application in Optical Modulation. *J. Mater. Chem.* **2010**, *20*, 7965–7969.
25. Ge, J. P.; Hu, Y. X.; Biasini, M.; Beyermann, W. P.; Yin, Y. D. Superparamagnetic Magnetite Colloidal Nanocrystal Clusters. *Angew. Chem., Int. Ed.* **2007**, *46*, 4342–4345.
26. Beydoun, D.; Amal, R.; Low, G. K. C.; McEvoy, S. Novel Photocatalyst: Titania-Coated Magnetite. Activity and Photodissolution. *J. Phys. Chem. B* **2000**, *104*, 4387–4396.
27. Lu, X. J.; Huang, F. Q.; Wu, J. J.; Ding, S. J.; Xu, F. F. Intelligent Hydrated-Sulfate Template Assisted Preparation of Nanoporous TiO_2 Spheres and Their Visible-Light Application. *ACS Appl. Mater. Interfaces* **2011**, *3*, 566–572.
28. Hansen, K. M.; Thundat, T. Microcantilever Biosensors. *Methods* **2005**, *37*, 57–64.
29. Joo, J.; Shim, J.; Seo, H.; Jug, N.; Wiesner, U.; Lee, J.; Jeon, S. Enhanced Photocatalytic Activity of Highly Crystallized and Ordered Mesoporous Titanium Oxide Measured by Silicon Resonators. *Anal. Chem.* **2010**, *82*, 3032–3037.
30. Liu, Y. J.; Li, X. X.; Zhang, Z. X.; Zuo, G. M.; Cheng, Z. X.; Yu, H. T. Nanogram per Milliliter-Level Immunologic Detection of Alpha-Fetoprotein with Integrated Rotating-Resonance Microcantilevers for Early-Stage Diagnosis of Heptocellular Carcinoma. *Biomed. Microdevices* **2009**, *11*, 183–191.
31. Lee, S.; Cho, J.; Lee, Y.; Jeon, S.; Cha, H. J.; Moon, W. K. Measurement of Hepatitis B Surface Antigen Concentrations Using a Piezoelectric Microcantilever as a Mass Sensor. *J. Sens.* **2012**, *2012*, 217958.
32. Hwang, K. S.; Lee, S. M.; Eom, K.; Lee, J. H.; Lee, Y. S.; Park, J. H.; Yoon, D. S.; Kim, T. S. Nanomechanical Microcantilever Operated in Vibration Modes with Use of RNA Aptamer as Receptor Molecules for Label-Free Detection of HCV Helicase. *Biosens. Bioelectron.* **2007**, *23*, 459–465.
33. Lee, S. M.; Hwang, K. S.; Yoon, H. J.; Yoon, D. S.; Kim, S. K.; Lee, Y. S.; Kim, T. S. Sensitivity Enhancement of a Dynamic Mode Microcantilever by Stress Inducer and Mass Inducer to Detect PSA at Low Picogram Levels. *Lab Chip* **2009**, *9*, 2683–2690.
34. Varshney, M.; Waggoner, P. S.; Montagna, R. A.; Craighead, H. G. Prion Protein Detection in Serum Using Micromechanical Resonator Arrays. *Talanta* **2009**, *80*, 593–599.
35. Varshney, M.; Waggoner, P. S.; Tan, C. P.; Aubin, K.; Montagna, R. A.; Craighead, H. G. Prion Protein Detection Using Nanomechanical Resonator Arrays and Secondary Mass Labeling. *Anal. Chem.* **2008**, *80*, 2141–2148.
36. Jin, R. C.; Cao, Y. C.; Hao, E. C.; Metraux, G. S.; Schatz, G. C.; Mirkin, C. A. Controlling Anisotropic Nanoparticle Growth Through Plasmon Excitation. *Nature* **2003**, *425*, 487–490.
37. Jin, R. C.; Cao, Y. W.; Mirkin, C. A.; Kelly, K. L.; Schatz, G. C.; Zheng, J. G. Photoinduced Conversion of Silver Nanospheres to Nanoprisms. *Science* **2001**, *294*, 1901–1903.
38. Turner, C. K.; Blieden, T. M.; Smith, T. J.; Feldon, S. E.; Foster, D. C.; Sime, P. J.; Phipps, R. P. A Novel ELISpot Method for Adherent Cells. *J. Immunol. Methods* **2004**, *291*, 63–70.
39. Wu, H.; Huo, Q. S.; Varnum, S.; Wang, J.; Liu, G. G.; Nie, Z. M.; Liu, J.; Lin, Y. H. Dye-Doped Silica Nanoparticle Labels/Protein Microarray for Detection of Protein Biomarkers. *Analyst* **2008**, *133*, 1550–1555.
40. Liang, K. Z.; Mu, W. J.; Huang, M. Y.; Yu, Z. X.; Lai, Q. K. Interdigitated Conductometric Immunosensor for Determination of Interleukin-6 in Humans Based on Dendrimer G4 and Colloidal Gold Modified Composite Film. *Electroanalysis* **2006**, *18*, 1505–1510.
41. Kapoor, R.; Wang, C. W. Highly Specific Detection of Interleukin-6 (IL-6) Protein Using Combination Tapered Fiber-Optic Biosensor Dip-Probe. *Biosens. Bioelectron.* **2009**, *24*, 2696–2701.
42. Wang, G. F.; Huang, H.; Zhang, G.; Zhang, X. J.; Fang, B.; Wang, L Dual Amplification Strategy for the Fabrication of Highly Sensitive Interleukin-6 Amperometric Immunosensor Based on Poly-Dopamine. *Langmuir* **2011**, *27*, 1224–1231.
43. Rowe, C. A.; Tender, L. M.; Feldstein, M. J.; Golden, J. P.; Scruggs, S. B.; MacCraith, B. D.; Cras, J. J.; Ligler, F. S. Array Biosensor for Simultaneous Identification of Bacterial, Viral, and Protein Analytes. *Anal. Chem.* **1999**, *71*, 3846–3852.
44. Chang, H. K.; Ishikawa, F. N.; Zhang, R.; Datar, R.; Cote, R. J.; Thompson, M. E.; Zhou, C. W. Rapid, Label-Free, Electrical Whole Blood Bioassay Based on Nanobiosensor Systems. *ACS Nano* **2011**, *5*, 9883–9891.